In *IEEE Transactions on Automatic Control,* 38(11), November 1993.

A Theoretical and Experimental Investigation of Explicit Force Control Strategies for Manipulators

Richard Volpe* and Pradeep Khosla†

Abstract

This paper presents a complete overview of basic strategies that have been proposed for force control of robot manipulators. First, the model of the plant to be controlled is reviewed. Next, the strategies are divided into force-based and position-based categories, according to previously reported implementations. Each of the controller types within these categories are analyzed, and predictions of stability and efficacy are made. Then it is shown that these two categories are actually the same, and this recognition leads to the concept of a novel second order low pass filter controller. Finally, all of the controllers are experimentally tested on the CMU DD Arm II , confirming the theoretical predictions. Among the important results presented is the conclusive demonstration for the first time that integral gain control is the best basic strategy for force control of manipulators.

1 Introduction

Many automation tasks require manipulators to interact with their environments. Necessary to the performance of these tasks are the basic capabilities of pushing, scraping, grinding, pounding, polishing, twisting, etc. All of these capabilities intrinsically require that the manipulator be force controlled. Two main approaches have been proposed for this purpose: *explicit force control* and *impedance control.* Since it has been demonstrated previously that an impedance controller with force feedback contains an explicit force controller [20, 23], the discussion in this paper is limited to explicit force control.

Explicit force control involves the direct command and measurement of force values, with the goal of having the output follow the input as closely as possible. Two types of explicit force control have been proposed: force-based, and inner position loop based. By far the most commonly discussed, the force-based techniques usually employ some form of

*Currently at The Jet Propulsion Laboratory, California Institute of Technology, Pasadena, California 91109. This work was completed while the author was a member of the Department of Physics, The Robotics Institute, Carnegie Mellon University, Pittsburgh, Pennsylvania, 15213

†Department of Electrical and Computer Engineering, The Robotics Institute, Carnegie Mellon University, Pittsburgh, Pennsylvania, 15213

PID control, as well as various simple forms of filtering. Inner position loop controllers, as the name suggests, have an outer force control loop that provides position commands to an inner position-based controller.

While many of these controllers have been analyzed before, this has not been done with an experimentally determined plant transfer function [20, 21]. As will be seen, erroneous conclusions about the stability of the system can result without a specific system model. Further, the analysis in this paper draws the force and position-based strategies together, into one coherent framework. This framework provides greater understanding of how gain variations affect stability, and suggests a new lowpass filter control technique.

The paper is organized as follows. First the plant model of the arm / sensor / environment system is reviewed. Then force-based explicit force control techniques will be presented and analyzed. Similarly, position-based explicit force control strategies will be presented and analyzed. It will then be shown how the two are the same, indicating which particular schemes will be most successful. Following this analysis, the experimental results will be presented for tests performed with each of the controllers discussed. Finally, conclusions are drawn from the analysis and experimentation.

2 Arm / Sensor / Environment Model

The physical system employed in this study is depicted in Figure 1. The environment is a cardboard box with an aluminum plate resting on it. The box is resting on a table that is considerably more stiff than the box, and is therefore considered ground for these tests. The force sensor is mounted on link six of the CMU DD Arm II . Attached to the force sensor is a steel probe with a brass weight on its end. The brass weight serves as an end effector substitute and provides a flat stiff surface for applying forces on the environment.

Previous analysis has indicated that a fourth order model of the arm / sensor / environment is necessary and sufficient for force control [5, 20]. This model is shown in Figure 2. The transfer function of this system is:

$$\frac{F_m}{F} = \frac{(m_B s^2 + c_3 s + k_3)k_2}{(m_B s^2 + (c_2 + c_3)s + (k_2 + k_3))(m_A s^2 + c_1 s + k_1) + (m_B s^2 + c_3 s + k_3)(c_2 s + k_2)} \tag{1}$$

where the measured force, F_m, is equal to $k_2(x_A - x_B)$. We have experimentally extracted parameter values for the components of this model, for the box/plate environment described. Theoretical and experimental details can be found elsewhere [21].

The pole/zero locations indicated by the extracted parameters differ greatly from those assumed by other researchers [5, 6]. Figure 3 shows all but the leftmost pole, which is at -28000 on the real axis. The complex pole pair (with real value ~ -12) is due mainly to the environment. The other pole pair (on the real axis) is due mainly to the sensor dynamics. These pole pairs will be called the environment and sensor poles, hereafter. It can be seen that the sensor poles are fairly far removed from the environmental ones, and are located farther into the left half plane. The leftmost sensor pole (at -28000) will be ignored.

3 Force-Based Explicit Force Control

Force based explicit force control describes a force controller that compares the reference and measured force signals, processes them, and provides an actuation signal directly to the plant. The reference force may also be fedforward and added to the signal going to the plant. Therefore, the general control diagram is shown in Figure 4, where G is the plant, H is the controller, R is the feedforward transfer function, and L is a force feedback filter. The plant G may be represented by the fourth order model discussed in the previous section. Active damping, if present, is included in G.

The controller H is usually some subset of PID control (i.e. P, I, PD, etc.). The simple form is chosen for two reasons. First, it is important to fully test and compare these simple controller forms to reveal their relative strengths and weaknesses. If the results are adequate, then more sophisticated nonlinear and adaptive techniques [8, 9, 16] need not be utilized. However, even if simple PID type control proves inadequate, a complete understanding of the behavior of the system under PID control is preliminary to understanding the analyzing the more sophisticated techniques.

The following sections present the specific forms of PID controllers tested. These schemes will be analyzed and the analytical results will be compared with previous results obtained by other researchers.

3.1 Strategies for Force-Based Explicit Force Control

This section presents the force-based explicit force control strategies that have been considered for this research. An extensive overview of strategies that have been considered by other researchers has been previously presented [29, 20, 24]. The strategies presented here are either a generalization of those, or selected because they are considered to be the most promising. In all cases, the joint torques commanded by these schemes are obtained through the transpose of the Jacobian, and gravity compensation is employed. The following notation is used: f_r is the reference force, f_m is the measured force, f is the control signal, $\dot{x}_m$ is measured velocity, K_{fp} is the proportional force gain, K_{fi} is the integral force gain, and K_{fd} is the derivative force gain. Finally , K_v is the velocity gain for the active damping employed. (In our experiments, the CMU DD Arm II has no intrinsic damping. Therefore, active damping was employed and included in the transfer function G, as previously mentioned.)

Proportional Control: [14, 10, 1, 5, 6, 32, 28, 2]

$$f = f_r + K_{fp}(f_r - f_m) - K_v \dot{x}_m \tag{2}$$

Integral Control: [18, 33, 3, 19, 31]

$$f = K_{fi} \int (f_r - f_m) dt - K_v \dot{x}_m \tag{3}$$

Proportional–Integral Control: [15, 13, 6]

$$f = K_{fp}(f_r - f_m) + K_{fi} \int (f_r - f_m) dt - K_v \dot{x}_m \tag{4}$$

Proportional–Derivative Control: [6, 30, 19]

$$f = f_r + K_{fp}(f_r - f_m) + K_{fd}\frac{d}{dt}(f_r - f_m) - K_v\dot{x}_m \tag{5}$$

Often, the force signal is very noisy and must be filtered before a derivative may be taken. Therefore, a simple dominant pole filter may be employed in the feedback path ($L = a/(s+a)$). The resultant control law in the Laplace domain is:

$$F(s) = F_r(s) + [K_{fp} + K_{fd}s]\left[f_r - \left(\frac{a}{s+a}\right) f_m\right] - K_v s X_m \tag{6}$$

3.2 Analysis of Force-Based Explicit Force Control

Given the wide spectrum of approaches and results reported in the literature, it is worthwhile to take a second look at these control strategies. Each will be analyzed below using the plant model previously developed.

3.2.1 Proportional Control

For proportional control, $H = K_{fp}$, and $L = 1$ in Figure 4. While the value of the feedforward term, R, does not affect the characteristic equation, a value different than unity will not cancel the reaction force from the environment, and the controller will not converge to the desired value. The feedforward term will be discussed further below. The closed loop transfer function with feedforward ($R = 1$) is:

$$\frac{F_r}{F_m} = \frac{(1 + K_{fp})G}{1 + K_{fp}G} \tag{7}$$

This is a Type 0 System and will have a nonzero steady-state error for a step input. The root locus of this system is shown in Figure 5. The corresponding Bode plot is shown in Figure 6.

As can be seen from the root locus, both the sensor poles and the environment poles move away from the real axis for increased proportional gain. Thus the system becomes more oscillatory. However, the environmental poles go to a pair of zeros, while the sensor poles go to infinity. Thus, the system may remain stable, but oscillations are likely to occur near the natural frequency of the environment. Further, note that the poles actually move into the right half plane, making the proportional gain controller unstable. This is contrary to the predictions of other researchers [6], which were based on a plant model that was not experimentally derived.

The Bode plot further illustrates this problem. There is a resonance peak from the environment dynamics, which corresponds to a normal mode of oscillation of the arm/environment system [21]. After this peak there is a 40 dB/decade drop-off which gives a minimum phase margin of $\sim 15°$ at $K_{fp} \approx 1$ [24].

The addition of a feedback lowpass filter, $L = \frac{a}{s+a}$, can reduce the magnitude of the resonance peaks. The corresponding closed loop transfer function becomes:

$$\frac{F_r}{F_m} = \frac{(R + K_{fp})G}{1 + K_{fp}(\frac{a}{s+a})G} \tag{8}$$

The root locus is modified by the presence of a pole on the real axis that moves left from $s = -a$. Depending on the magnitude of a, this pole can reduce the response of the resonance peak. For $a \rightarrow \infty$ this becomes a pure proportional controller. For $a \rightarrow 0$ this scheme is very similar to integral control, discussed below. (For this reason, an implementation of filtered proportional control will not be presented in this paper.) Improved response with lowpass filtering has been reported [1].

Finally, we have shown elsewhere that the proportional force gain may theoretically be as low as negative one [23]. The modified root locus, for gains $-1 \leq K_{fp} < \infty$, is shown in Figure 7. In this figure the poles are shown at the beginning of the root locus, where $K_{fp} = -1$. Comparing Figures 7 and 5 it can be seen that negative gains provide a very stable system. Gains in this region have proven very effective for impact control [22, 26].

3.2.2 Integral Control

For integral control, $H = \frac{K_{fi}}{s}$, and $L = 1$ in Figure 4. A nonzero feedforward term, R, yields the following transfer function:

$$\frac{F_r}{F_m} = \frac{(R + \frac{K_{fi}}{s})G}{1 + \frac{K_{fi}}{s}G} \tag{9}$$

Letting R be unity places a closed loop zero at $s = -K_{fi}$ which limits the effectiveness of the integrator pole. Also, a feedforward signal is not necessary since the integrator will eliminate any steady state error for a constant input. Therefore, R is set to zero and the transfer function is:

$$\frac{F_r}{F_m} = \frac{\frac{K_{fi}}{s}G}{1 + \frac{K_{fi}}{s}G} \tag{10}$$

This is a Type 1 System and has a finite error to a ramp input. The root locus of this system is shown in Figure 8. The corresponding Bode plot is shown in Figure 9.

As can be seen in the root locus plot, the introduction of the integral pole moving to the left causes the environmental and sensor poles to move right. This has been previously viewed as destabilizing [6]. In the previous section, the sensor poles caused this same behavior from a proportional controller. The two root loci are compared in Figure 10. As can be seen, the loci are similar except that the integral controller has the benefit of a dominant low pass pole on the real axis. The Bode plot indicates that the low pass nature of integral control hides the resonance spikes well below unity magnitude. The point of zero phase margin indicates a maximum integral gain, $K_{fi} \approx 28$ [24].

3.2.3 Proportional–Integral Control

A PI controller is a linear combination of the above two schemes. In this case, $H = K_{fp} + \frac{K_{fi}}{s}$, $L = 1$, and for reasons mentioned above, $R = 0$. Therefore, the transfer function is:

$$\frac{F_r}{F_m} = \frac{\left(K_{fp} + \frac{K_{fi}}{s}\right) G}{1 + \left(K_{fp} + \frac{K_{fi}}{s}\right) G} \tag{11}$$

Obviously, the behavior is a combination of the behaviors of pure proportional and pure integral control. The appearance of the root locus and Bode plot will depend on the gain which is varied.

3.2.4 Proportional–Derivative Control

A PD controller includes a derivative term with the proportional control discussed above. In this case, $H = K_{fp} + sK_{fd}$, $L = 1$, and for reasons mentioned above, $R = 1$. Therefore the transfer function is:

$$\frac{F_r}{F_m} = \frac{(R + K_{fp} + K_{fd}s)G}{1 + (K_{fp} + K_{fd}s)G} \tag{12}$$

Choosing a specific value of K_{fp} with $K_{fd} = 0$ will determine the starting place of the root locus of K_{fd}. This starting place will be somewhere on the root locus of K_{fp} in Figure 5. Independent of the starting point the root locus will have similar characteristics. For K_{fp} large, the derivative term will have no influence, so the controller and its root locus can be approximated as those for proportional control alone. For $K_{fp} = 0$ this scheme will reduce to pure derivative control which will not follow the reference force. However, the transfer function and associated root locus for $K_{fp} = 0$ represent the extreme of the behavior for a PD controller. Just as the behavior of PI control was intuited from that of P and I control alone, the behavior of PD control can be best understood by studying its extremes of pure proportional and pure derivative control. Thus, K_{fp} is considered zero in the following discussion. The resulting root locus is shown in Figure 11. The corresponding Bode plot is shown in Figure 12.

As can be seen in the root locus plot, for a certain range of gains, derivative control moves all of the poles further left, thus appearing to make the system more stable. For this reason, PD control has been predicted to be very stable [6].

However, the Bode plot of the system shows a major problem with this approach. Derivative control acts as a band pass filter, amplifying noise and oscillations at the resonant frequency. This surely will drive an underdamped system into oscillation.

Another implementational factor must be considered with respect to derivative control. Typically, the feedback signal from a force sensor is very noisy. One example can be seen in Figure 20. Taking the derivative of such a signal is not advisable. However, filtering may be effective. Passive filtering may be accomplished by the use of a compliant sensor or sensor cover [1, 30]. However, this method can introduce uncontrolled degrees of freedom into the system, or reduce the effective force that may be applied. Alternatively, active filtering may be used. This will be discussed next.

3.2.5 Filtered Proportional–Derivative Control

To filter the force signal a dominant pole filter may be used, placing the transfer function $L = \frac{a}{s+a}$ in the feedback path. Therefore the transfer function becomes:

$$\frac{F_r}{F_m} = \frac{(R + K_{fp} + K_{fd}s)G}{1 + (K_{fp} + K_{fd}s)\left(\frac{a}{s+a}\right)G} \tag{13}$$

As before, K_{fp} is chosen to be zero for this analysis. Choosing $a \to \infty$ will not make an effective filter of the high frequency noise. Choosing $a \to 0$ will make this a proportional gain controller. Proportional gain control has already been shown to be ineffective in masking the resonance oscillation of the system.

For the case of nonzero K_{fp} and $a \to 0$, the characteristic equation becomes that of a PI controller. As discussed before, the response of this controller will be between that of P and I control alone.

3.3 Discussion of Forced-Based Explicit Force Control

It seems apparent from the above analysis that explicit force control with the experimentally determined plant is best accomplished by integral control. First, the integral controller is a Type 1 System and will have zero steady-state error for a constant reference force. Second, an integral controller acts as a low pass filter, reducing the chance of resonance oscillations occurring in the system. This is deemed to be very important. Higher order modes of oscillation can cause the assumed model to become invalid and actually make the system nonlinear, especially if separation from the environment occurs.

One of the main arguments against integral control is that it does not permit fast force trajectory tracking. However, this goal is simply not achievable for a manipulator that is not mechanically attached to the environment. A simple argument should demonstrate this point. Consider a manipulator that is pressing on a surface with a natural frequency of oscillation. Between the manipulator and the surface there is no physical compliance. Consider also that the manipulator is to reduce its applied force. If the rate of the reduction is greater than the natural frequency of the environment then contact will be lost. In other words, the arm will pull away faster than the environment can respond. Lost contact can cause instability to develop and should be avoided. Therefore, it can be simply put that *the force control response time is limited by the environmental dynamics.* This is seen directly in the integral control root locus and Bode plots above, Figures 8 and 9. The limiting value of K_{fi} obtained from the phase margin [24] places the integral pole just to the right of the environmental poles.

4 Position-Based Explicit Force Control

A second class of explicit force controllers consists of those based on an inner position loop [11, 4, 7]. These controllers were probably implemented first for practical reasons — most commercial manipulators have built in position controllers and don't allow direct access to actuator torques. As shown in Figure 13, the outer force loop provides a reference position to the inner position loop. In this diagram, W is the position controller which is typically a PD controller:

$$W = K_p + K_v s \tag{14}$$

The reference force is transformed into a reference position through an admittance, which is described as the inverse of a second order impedance, Z, where:

$$Z = m_f s^2 + c_f s + k_f \tag{15}$$

Again the joint torques are obtained from the Cartesian forces through the transpose of the Jacobian, and gravity compensation is employed. The plant damping is again provided actively by the velocity gain K_v.

A review of position-based force control implementations that have been performed by other researchers is given elsewhere [29, 20]

4.1 Analysis of Position-Based Explicit Force Control

4.1.1 Ensuring a Type 1 System

As has been stated previously, a Type 1 system is desirable because it has zero steady-state error to a constant input. Previous analysis of the position-based controllers, especially that of DeSchutter, indicates the need to consider controllers that must become Type 1 Systems [4]. The previous work, coupled with the plant model developed in this paper, indicates a new and novel way in which to view inner position loop-based explicit force control. As will be seen, the previously reviewed force-based explicit force controllers are actually a subset of this strategy.

Consider first the position-based force controller that uses velocity as well as position feedback ($W = K_p + K_v s$). Deschutter's results indicate that the outer force controller providing reference positions must have at least one free integration. To achieve this the force controller must be $Z = s(m_f s + c_f)$. This is essentially a second order low pass filter. Contrary to this is the first order low pass filter which will have a nonzero steady state error [7].

Next, consider the position-based force controller that uses only velocity feedback ($W = K_v s$). For this scheme, the outer force loop must provide a reference velocity, as well as satisfy the criterion of at least one free integration. This implies $Z = m_f s^2$. Notice that this scheme is exactly what has previously been considered as integral gain explicit force control with active damping. Viewed in this way, the velocity feedback is not just added to improve damping. Instead, it is part of a inner loop, position-based, feedback controller.

Finally, the third case of no inner loop reduces to the second case since the transfer function of the arm, sensor and environment does not change form when the active damping is removed. This is because velocity 'feedback' is still present in the system in the form of natural damping.

4.1.2 Position-Based Explicit Force Control Viewed as Force-Based Explicit Force Control

Having shown the correspondence between position-based and force-based explicit force control, it is possible to change the first into the second. Consider separating the position controller in Figure 13 into two parts, W_1 and W_2. Figure 14 shows the resultant controller block diagram.

It can now be seen that the inner loop simply adds stiffness and damping to the plant. Since the plant already contains active damping [21], this component of W_2 is superfluous. The position gain, on the other hand, is completely undesirable. It increases the manipulator stiffness, which is added directly to the environmental stiffness in the plant transfer function, making the system more oscillatory. Therefore, *position-based force control differs from* *force-based force control by the addition of stiffness to the plant. Further, this additional stiffness is destabilizing.*

The outer loop of the position-based force control can be shown to assume the form of any of the force-based explicit force controllers previously discussed. Consider the form of the controller shown in Figure 14. It is apparent that the controller now has a form previously associated with force-based explicit force control, where

$$H = \frac{W_1}{Z} = \frac{K_p + K_v s}{m_f s^2 + c_f s + k_f} \tag{16}$$

Notice that all of the explicit force controllers can be constructed from this transfer function:

Proportional Control	$K_{fp} = K_p/k_f \quad K_v = m_f = c_f = 0$
Proportional Control	$K_{fp} = K_v/c_f \quad K_p = m_f = k_f = 0$
Integral Control	$K_{fi} = K_p/c_f \quad K_v = m_f = k_f = 0$
Integral Control	$K_{fi} = K_v/m_f \quad K_p = c_f = k_f = 0$
Derivative Control	$K_{fd} = K_v/k_f \quad K_p = m_f = c_f = 0$
PI Control	$K_{fp} = K_v/c_f, K_{fi} = K_p/c_f \quad m_f = k_f = 0$
PD Control	$K_{fp} = K_p/k_f, K_{fd} = K_v/k_f \quad m_f = c_f = 0$
Filtered P Control	$K_{fp}/(s + a) = K_p/(c_f s + k_f) \quad K_v = m_f = 0$
Filtered PD Control	$(K_{fp}+K_{fd}s)/(s+a) = (K_p+K_v s)/(c_f s+k_f) \quad m_f = 0$
2$^{\text{nd}}$ Order Low Pass Filter	$K_{fp}/(s(s + a)) = K_p/(s(m_f s + c_f) \quad K_v = k_f = 0$

The only new controller in this list is the second order lowpass filter. It will be discussed in the next section.

4.1.3 Root Locus and Bode Plots

As has been discussed above, the second order low pass filter is the only controller form that is newly introduced by the concept of position-based explicit force control. It is worthwhile to look at the root locus and Bode plot for this scheme. Like the first order dominant pole introduced by low pass filtering or integral control, the two poles introduced by a second order filter should be placed to the right of the environment poles. Since the controller has been chosen to be Type 1, one of the poles is constrained to begin its locus at the origin. Thus the other should begin to the left of the environmental poles. As the gain is increased, the filter poles on the real axis will come together and give a double pole filter just to the right of the environmental poles. A root locus for $a = 20$ is shown in Figure 15. The corresponding Bode plot is shown in Figure 16.

Unlike integral gain control, these two filter poles can leave the real axis. Thus, oscillations in the system may be result. If the filter poles leave the real axis to the right of the environmental poles, the frequency and decay of the oscillations will be dominated by the filter poles. In this case, the characteristics of the oscillations may noticeably differ from those seen for proportional or integral gain control.

5 Analytical Conclusions and Experimental Predictions

Thus far we have presented a stability analysis of various explicit force control routines using the experimentally derived plant model. This work is unique in its broad coverage of control strategies and use of an experimentally determined plant model. The results of this work also contradict the predictions of other researchers [6] in that integral control is apparently best, and PD control worst.

The analysis indicates that integral control is the best choice for explicit force control for several reasons: a simple form, intrinsic lowpass filtering, and zero steady state error for a constant reference force. A possible second choice is the second order lowpass filter. Although, slightly more complicated than simple integral control it promises to filter the force oscillations better. Proportional control is the third choice. However, with this controller the dominant poles are complex, indicating that oscillations will occur even for low gains. Further, the analysis shows that proportional gain control becomes unstable, which has not been predicted previously. Finally, any control using the derivative of the force signal does not seem promising. This type of controller will act as a band pass filter at the natural frequency of the system. Also, obtaining a good derivative of the force signal may prove difficult.

The rest of this paper presents the data obtained from the implementation of the explicit force control strategies discussed. All experiments were performed with the CMU DD Arm II and implemented under the Chimera II real time operating system [17] with the computer architecture described elsewhere [20]. This experimental review of force control methodologies is unique in its breadth, since a complete spectrum of strategies has been implemented on the same system. The commonality amongst the experiments has permitted the ability to objectively compare and contrast these strategies, and draw conclusions about the efficacy of each. As will be seen, the results support the previous analysis and show the superiority of integral force control for force trajectory tracking.

First, data collected from explicit force control strategies is presented. These include proportional control with feedforward, integral control, and proportional–derivative control. All of these tests were conducted using the environment modelled previously. The contact problem was ignored to simplify these tests, but we have studied it extensively elsewhere [22, 26]. Finally, results are presented from tests conducted with the best of these controllers on a very stiff environment.

6 Explicit Force Control

This section presents the results of implementing the explicit force control schemes discussed. All of these schemes were implemented in a Hybrid Control framework [12] in which the force was controlled in one direction (world frame z axis), and all other directions were position controlled. To be consistent with the arm / sensor / environment model developed, active damping was provided ($K_v = 10$) in the force controlled direction [21, 25]. The control rate was 300 Hz. The chosen reference force trajectory has steady state, step, and ramp components and is shown as a dashed curve in all of the graphs. The measured force response of the system is shown as a solid curve.

6.1 Proportional Gain with Feedforward Control

The first controller to be discussed is proportional gain force control with the reference force fedforward. The exact form of the control law used is:

$$\tau \; = \; J^T \, [\, f_r + K_{fp}(f_r - f_m) \; - \; K_v \dot{x}_m] \; + \; g. \tag{17}$$

Figures 17 (a) through (h) show the response of this controller to the reference force trajectory. There are several things to note about the response profiles to variations in the proportional gain. First, as predicted by the model, the system exhibits the characteristics of a Type 0 system: finite steady state error for a step input and unbounded error for a ramp input. Second, for an increase in position gain, the steady state error reduces, but at the cost of increasingly larger overshoot. As correctly predicted, this control scheme causes instability at $K_{fp} \approx 1$. Also, the fact that the environmental poles are always off the real axis can be seen in the steady state oscillations that occur at the system's natural frequency ($\sim$ 15 Hz), particularly after the step input. Finally, it can be seen that negative proportional gains are increasingly more stable, but the response of the system approaches zero as $K_{fp} \to -1$.

One possible method of improving the steady state error of this controller is to increase the feedforward signal by a factor that would make that error small for the open loop case ($K_{fp} = 0$). Figure 17 (d) shows that a feedforward term of approximately 1.4 f_r would be necessary. This, however, would not eliminate the oscillations that are present, especially after the step input.

6.2 Integral Gain Control

Integral explicit force control was implemented with the following form of control law:

$$\tau \; = \; J^T \left[K_{fi} \int (f_r - f_m) dt \; - \; K_v \dot{x}_m \right] \; + \; g. \tag{18}$$

where g is the gravitational torque. Figures 18 (a) through (e) show the response of this controller to the reference force trajectory. The most notable aspect of this controller is the dominance of the integrator pole on the real axis for low gains. This causes the system to be Type 1, as is apparent from the zero steady state error to the step input and constant error to the ramp input. As predicted, this pole acts as a low pass filter until it moves past the environment poles. This happens gradually as the gain increases past $K_{fi} \approx 10$ as shown in the center of the root locus diagram of Figure 8. Also predicted by that model is that the system becomes unstable for gains near $K_{fi} = 30$. The real system is not unstable until K_{fi} reaches the upper thirties, which implies a small modelling error. Also, the model previously presented does not explain the nonlinear response seen for $K_{fi} = 37.5$. For a linear system, the envelopes of the two dominant oscillations would be the same, which is obviously not the case. This limitation of the model is not significant, since it does not manifest itself within the desirable operating range of this controller.

6.3 PD Control

Proportional / Derivative control was also implemented. Simple differencing of the measured force signal to obtain the derivative was unsuccessful because of the extremely noisy nature of the force signal. Therefore, the force feedback signal was lowpass filtered by using the transfer function $L = a/(s + a)$ in the feedback path in Figure 4. The reference signal is not filtered. Therefore, the implemented control law in the Laplace domain is:

$$\tau(s) = J^T \left\{ F_r(s) + [K_{fp} + K_{fd}s] \left[F_r(s) - \left(\frac{a}{s+a}\right) F_m(s) \right] + K_v s\, X(s) \right\} + g(s). \quad (19)$$

Figure 19 shows the response of the system, as well as the reference force and filtered force (long dash curve), for $K_{fp} = 0.5$, $K_{fd} = 0.01$, and $a = 10$. The results are not much better than for proportional gain alone. As will be reviewed below, improvements in the performance of this controller can not be made by varying the gains given here [27].

First, increasing the derivative gain does not improve the response of the system because the amplified low frequency noise can still drive the system unstable. While Figure 19 seems to show a fairly smooth filtered force signal, Figure 20 shows a closer view of a section of the curve. Obviously, much of the noise has been removed, but some still remains. With a large enough gain the noise will dominate. Moving the filter pole to the right ($a < 10$) will eliminate this noise, but it introduces a more serious problem of lag.

Figure 21 shows that the calculated derivative (solid curve) appears accurate. (The dashed curve is the measured force.) However, it is apparent from this figure and Figure 19 that there is lag introduced by the filtering process. This lag becomes extremely important when it is comparable to the period of oscillation of the system. Figure 22 shows the original force signal (solid), the filtered force signal (short dash), and the derivative of the filtered signal (long dash). For this oscillation frequency, the filtering process causes the filtered force to lag the measured force by one quarter cycle. This makes the force signal 180° out of phase with the ideal derivative signal. Thus, the proportional gain acts as a destabilizing negative derivative gain. Further, the derivative of the filtered signal leads it by one quarter cycle. Thus, the derivative is in phase with the originally measured force and the derivative gain acts as a proportional gain. Increasing the derivative gain causes greater oscillations exactly when the effective damping is being reduced by the proportional gain. This obviously will cause the system to go unstable.

It can be concluded from this discussion than the filter pole should be significantly larger than the natural frequency of the system, However, it also must be small enough to effectively filter the noise of the force sensor. These two criteria could not be met with our system. To be fair, most systems will never meet this criteria. Force controlled systems are most challenged by stiff environments that have high natural frequencies. It is unlikely that a sensor can be built that has noise only at frequencies much greater than the natural frequencies of these environments.

One solution, however, is to use a soft force sensor or compliant covering on the sensor. The compliance acts as a lowpass filter with no time delay. In this way, the derivative of the force signal may be used under the condition that the time necessary to calculate it is not significant. In this case, without a noisy force signal, simple differencing of the current and most recent force samples will usually suffice. Thus, all that is required is that the force sampling frequency is not of the same order of magnitude as the natural frequency of the system. Successful PD force control with a soft force sensor has been reported elsewhere [30].

6.4 Second Order Low Pass Filter Control

As discussed in Section 4.1.1, a second order low pass filter controller has been implemented. The following control law was used:

$$\tau(s) = J^T \left[\frac{K_{fp}}{s(s+a)} (F_r(s) - F_m(s)) + K_v s\, X(s) \right] + g(s). \tag{20}$$

Figures 23 show the response of this system for three distinct regions of operation: filter poles meeting on the real axis to the right of, near, and to the left of the environment poles. This behavior was previously shown near the origin in Figure 15.

Figures 23 (a) through (c) show the response for $a = 15$ and increasing gain K_{fp}. Referring to the root locus near the origin in Figure 15, it can be see that the rightmost pole dominates in (a), until the two poles on the real axis meet in (b), and then leave the real axis in (c). For the small gain case, the dominant pole acts much like the single pole of the integral controller presented previously. Because a is small, the filter poles meet to the right of the environmental poles and dominate the response for low frequencies. Notice that the oscillations present in (c) are not close to the natural frequency of the environment, as was true with the previous controller results presented.

Figures 23 (d) through (f) show the response for $a = 45$ and increasing gain K_{fp}. Again, the three graphs refer to the poles spread on the real axis (d), together on the real axis (e), and off the real axis (f). The filter pole dominates for low gains, making the response look like integral control. The response continues to look like integral control as the poles meet in the vicinity of the environmental poles (e). Figure 23 (e) shows the best response obtained with this controller. In (f) the poles have again moved off the real axis, as indicated by the oscillations.

Finally, Figures 23 (g) through (i) show the response for $a = 180$ and increasing gain K_{fp}. The three graphs refer to the poles spread on the real axis (g), together on the real axis (h), and off the real axis (i). Again, the first two graphs look much like integral control. However, this time the third graph also looks like integral force control with gain that is too high. This is intuitively correct since the meeting point of the filter poles for such a high value of a is to the left of the environment poles. Thus, the right filter pole acts like the integral control pole until it is moves far to the left of the environment poles, at which point its influence is negligible. The influence of the second filter pole remains negligible throughout.

Thus, it can be concluded that this control scheme is only marginally better than integral control. While the double pole on the real axis promises to be a better low pass filter, its location must still be close to the real axis projection of the environmental poles to minimize lag. This placement reduces its ability to better suppress the oscillation of the system. Further, this controller is much more difficult to tune since it requires the adjustment of two parameters instead of one. For these reasons it is not preferable to pure integral control. However, this implementation does successfully demonstrate that position-based explicit force control, as discussed in Section 4.1.1, is stable and useful.

7 Results with a Stiff Steel Environment

All of the results presented previously were obtained with the environment modelled reviewed earlier in this paper and described in detail elsewhere [20, 21]. To further test the proportional and integral gain controllers, a very rigid steel pedestal was also used as the environment. This pedestal was made from one inch thick steel: two 1 foot square plates at both ends of a cylinder 34 inches long and 8 inches in diameter. The bottom plate was bolted to a concrete floor. Another piece of steel was bolted to the top plate. It consisted of two 6 by 1/4 inch steel plates joined at right angles. (This is commonly called 'angle iron'.) The angle iron was 1 foot long and provided a vertical surface to press.

Two points on this pedestal were used for force trajectory experiments. The first was on the top surface (z direction), directly above the wall of the supporting column. It was the most rigid point on the structure. The pedestal was mounted such that this spot was very close to the Cartesian position at which all previous experiments were performed. The second spot on the pedestal used for experiments was on the face of the angle iron (x direction). This was much less stiff but still considerably more stiff than the previously modelled environment. Its reduction in stiffness from the top surface was due to flexion of the column and weaknesses in the bolted connections.

First proportional gain control was tried at the two test points on the pedestal. Figures 24 show the response for the highest proportional gains used in the z direction. For this stiff direction, the gain is stable even for $K_{fp} = 2$. Figures 25 show the response for the highest proportional gains used in the x direction. It is apparent that general behavior of the controller is the same as before for the modelled environment. However, it can also be seen that a stiffer environment permits higher proportional force gains.

Next integral gain control was tried at the two test points on the pedestal. Figures 26 show the response for the highest integral gains used in the z direction. Figures 27 show the response for the highest integral gains used in the x direction. For both directions, the gain is still stable for $K_{fi} = 50$. It is apparent that general behavior of this controller is also the same as before with the modelled environment. However, it can also be seen that a stiffer environment again permits higher gains.

The major conclusion to draw from this data is that all of the discussions and results from the analysis of the modelled system carry over to a very stiff environment. In this case it can be assumed that most of the dynamics of the system are within the manipulator and the sensor. Therefore, an infinitely stiff environment (if one could be found) would not provide much different results.

8 Conclusion

This paper has presented the analysis and experimental testing of a broad spectrum of basic force control strategies: proportional with feedforward, integral, filtered feedback proportional–derivative, and second order low pass filtering. The data permits several important conclusions. First, force trajectory tracking is best accomplished with integral gain explicit force control. Second, PD force control and damping strategies should not be relied on to provide stability to the system when in contact with the environment, since it is impossible to obtain a true derivative. Finally, the fourth order model of the environment previously obtained through experimentation was further validated by the correct predictions of system behavior that it provided.

While integral control has been utilized by many researchers, this work is unique in that the efficacy of integral control has never been experimentally demonstrated against the full spectrum of basic control strategies.

9 Acknowledgements

This research was performed at Carnegie Mellon University and supported by an Air Force Graduate Laboratory Fellowship (for Richard Volpe), DARPA under contract DAAA-21-89C-0001, the Department of Electrical and Computer Engineering, and The Robotics Institute.

The writing and publication of this paper was supported by the above and the Jet Propulsion Laboratory, California Institute of Technology, under a contract with the National Aeronautics and Space Administration.

The views and conclusion contained in this document are those of the authors and should not be interpreted as representing the official policies, either expressed or implied, of the U.S. Air Force, DARPA, or the U.S. Government. Reference herein to any specific commercial product, process, or service by trade name, trademark, manufacturer, or otherwise, does not constitute or imply its endorsement by the United States Government or the Jet Propulsion Laboratory, California Institute of Technology.

References

[1] C. An and J. Hollerbach. Dynamic Stability Issues in Force Control of Manipulators. In *Proceedings of the IEEE Conference on Robotics and Automation*, pages 890–896, 1987.

[2] R. Anderson and M. Spong. Hybrid Impedance Control of Robotic Manipulators. *IEEE Journal of Robotics and Automation*, 4(5):549–556, October 1988.

[3] E. Colgate and N. Hogan. An Analysis of Contact Instability In Terms of Passive Physical Equivalents. In *Proceedings of the IEEE Conference on Robotics and Automation*, pages 404–409, 1989.

[4] J. De Schutter. A Study of Active Compliant Motion Control Methods For Rigid Manipulators Based on a Generic Scheme. In *Proceedings of the IEEE Conference on Robotics and Automation*, pages 1060–1065, 1987.

[5] S. Eppinger and W. Seering. On Dynamic Models of Robot Force Control. In *Proceedings of the IEEE Conference on Robotics and Automation*, pages 29–34, 1986.

[6] S. Eppinger and W. Seering. Understanding Bandwidth Limitations on Robot Force Control. In *Proceedings of the IEEE Conference on Robotics and Automation*, pages 904–909, Raleigh, N.C., 1987.

[7] H. Ishikawa, C. Sawada, K. Kawase, and M. Takata. Stable Compliance Control and Its Implementation for a 6 D.O.F. Manipulator. In *Proceedings of the IEEE Conference on Robotics and Automation*, pages 98–103, 1989.

[8] Slotine J. and W. Li. Adaptive Strategies in Constrained Manipulation. In *Proceedings of the IEEE International Conference on Robotics and Automation*, pages 595–601, April 1987.

[9] H. Kazerooni and T. Tsay. Stability Criteria for Robot Compliant Maneuvers. In *Proceedings of the IEEE Conference on Robotics and Automation*, pages 1166–1172, April 24-29 1988.

[10] O. Khatib and J. Burdick. Motion and Force Control of Robot Manipulators. In *Proceedings of the IEEE Conference on Robotics and Automation*, pages 1381–1386, 1986.

[11] J. Maples and J. Becker. Experiments in Force Control of Robotic Manipulators. In *Proceedings of the IEEE Conference on Robotics and Automation*, pages 695–702, 1986.

[12] M. Mason. Compliance and Force Control for Computer Controlled Manipulators. *IEEE Transactions on Systems, Man, and Cybernetics*, 11(6):418–432, June 1981.

[13] F. Miyazaki and S. Arimoto. Sensory Feedback for Robot Manipulators. *Journal of Robotic Systems*, 2(1):53–71, 1985.

[14] R. Paul and C. Wu. Manipulator Compliance Based on Joint Torque. In *IEEE Conference on Decision and Control*, pages 88–94, New Mexico, 1980.

[15] M. Raibert and J. Craig. Hybrd Position/Force Control of Manipulators. *Journal of Dynamic Systems, Measurement, and Control*, 103(2):126–133, June 1981.

[16] Venkataraman S. and Gulati S. Control of Nonlinear Systems Using Terminal Sliding Modes. In *Proceedings of the American Control Conference*, Chicago, Ill., June 24-26 1992.

[17] D. Stewart, D. Schmitz, and P. Khosla. Implementing Real-Time Robotic Systems Using Chimera II. In *Proceedings of the IEEE International Conference on Robotics and Automation*, pages 598–603, May 1990.

[18] W. Townsend and J. Salisbury. The Effect of Coulomb Friction and Stiction on Force Control. In *Proceedings of the IEEE Conference on Robotics and Automation*, pages 883–889, 1987.

[19] D. Vischer and O. Khatib. *Design and Development of Torque-Controlled Joints*, pages 271–286. Springer-Verlag Berlin Heidelberg, 1990.

[20] R. Volpe. *Real and Artificial Forces in the Control of Manipulators: Theory and Experiments*. PhD thesis, Carnegie Mellon University, Department of Physics, September 1990.

[21] R. Volpe and P. Khosla. Theoretical Analysis and Experimental Verification of a Manipulator / Sensor / Environment Model for Force Control. In *Proceedings of the IEEE International Conference on Systems, Man, and Cybernetics*, Los Angeles, November 1990.

[22] R. Volpe and P. Khosla. Experimental Verification of a Strategy for Impact Control. In *Proceedings of the IEEE International Conference on Robotics and Automation*, Sacramento, CA, April 1991.

[23] R. Volpe and P. Khosla. The Equivalence of Second Order Impedance Control and Proportional Gain Explicit Force Control: Theory and Experiments. In *Proceedings of the Second Annual International Symposium on Experimental Robotics*, Toulouse, France, June 1991.

[24] R. Volpe and P. Khosla. An Analysis of Manipulator Force Control Strategies Applied to an Experimentally Derived Model. In *Proceedings of the IEEE/RSJ International Conference on Intelligent Robots and Systems*, Raleigh, North Carolina, July 7-10 1992.

[25] R. Volpe and P. Khosla. An Experimental Evaluation and Comparison of Explicit Force Control Strategies for Robotic Manipulators. In *Proceedings of the American Control Conference*, Chicago, Ill., June 24-26 1992.

[26] R. Volpe and P. Khosla. A Theoretical and Experimental Investigation of Impact Control for Manipulators. In *International Journal of Robotics Research*, (accepted for publication in 1993).

[27] R. Volpe and P. Khosla. Computational Considerations in the Implementation of Force Control Strategies. In *Journal of Intelligent and Robotic Systems: Theory and Applications. Special Issue on Computational Aspects of Robot Kinematics, Dynamics, and Control*, (accepted for publication in 1993).

[28] D. Wedel and Saridis G. An Experiment in Hybrid Position/Force Control of a Six DOF Revolute Manipulator. In *Proceedings of the IEEE Conference on Robotics and Automation*, pages 1638–1642, 1988.

[29] D. Whitney. Historical Perspective and State of the Art in Robot Force Control. In *Proceedings of the IEEE Conference on Robotics and Automation*, pages 262–268, 1985.

[30] Y. Xu and R. Paul. On Position Compensation and Force Control Stability of a Robot with a Compliant Wrist. In *Proceedings of the IEEE Conference on Robotics and Automation*, pages 1173–1178, 1988.

[31] T. Yoshikawa. Dynamic Hybrid Position/Force Control of Robot Manipulators — Description of Hand Contraints and Calculation of Joint Driving Force. *IEEE Journal of Robotics and Automation*, RA-3(5):386–392, October 1987.

[32] K. Youcef-Toumi. Force Control of Direct-Drive Manipulators For Surface Following. In *Proceedings of the IEEE Conference on Robotics and Automation*, pages 2055–2060, 1987.

[33] K. Youcef-Toumi and D. Gutz. Impact and Force Control. In *Proceedings of the IEEE Conference on Robotics and Automation*, pages 410–416, 1989.

List of Figures

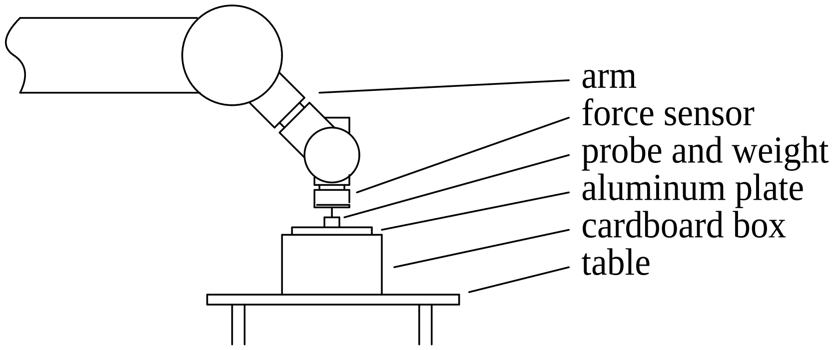

Figure 1: Experimental setup for force control experiments.

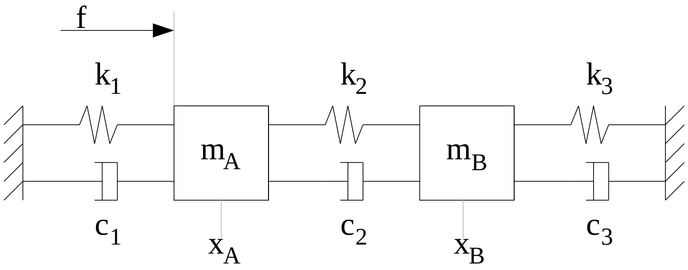

Figure 2: General fourth order model of arm, sensor, and environment system.

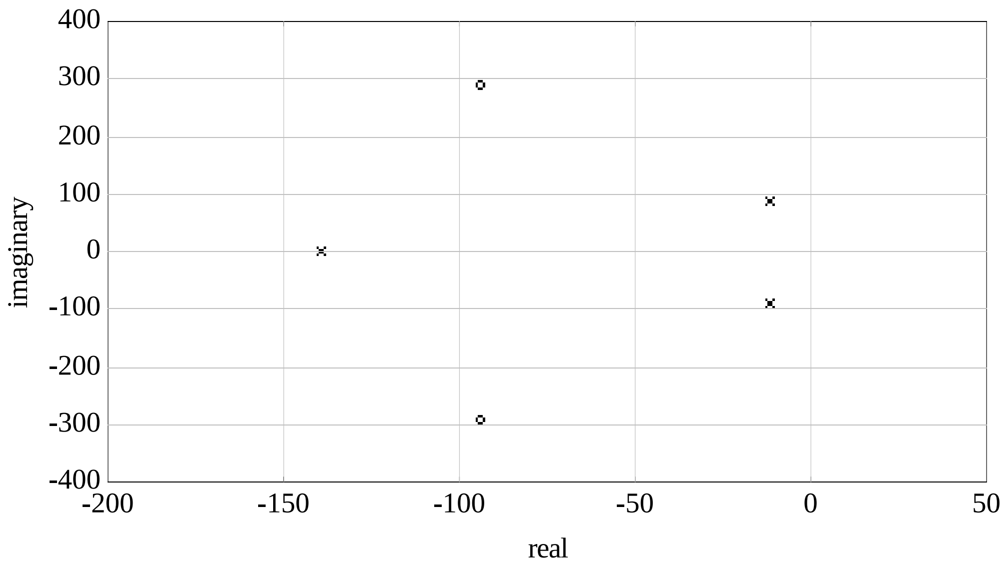

Figure 3: The pole and zero locations for the fourth order model, using the experimentally extracted parameters. Not shown is the leftmost pole which is at -28000 on the real axis.

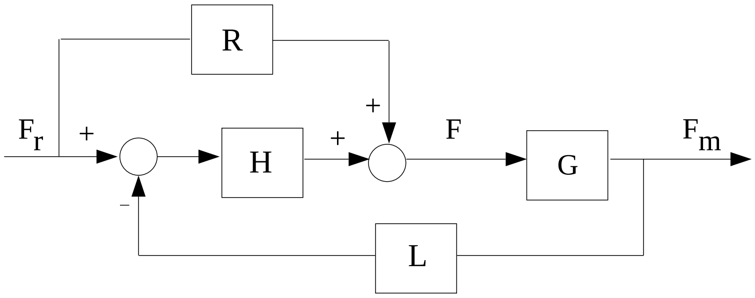

Figure 4: Block diagram of a generic force-based, explicit force controller.

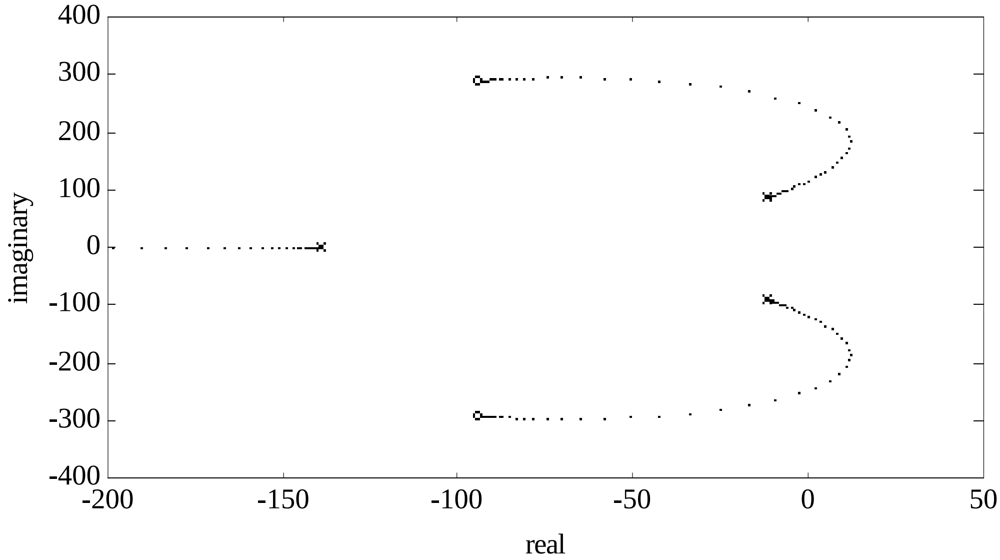

Figure 5: Root locus for the fourth order model under proportional gain explicit force control. The locus first crosses the imaginary axis for $K_{fp} \approx 1.2$.

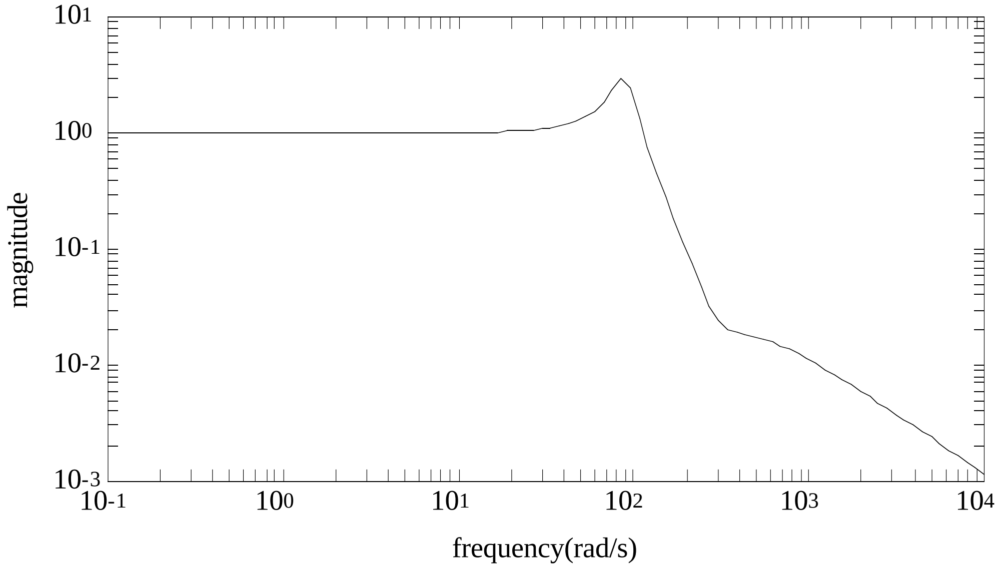

Figure 6: Bode plot for the fourth order system under proportional gain explicit force control. The resonance peak occurs near the natural frequency of the environment. The gain margin is 1.2 at ω = 118rad/s, which corresponds to the root locus crossing to the right half plane in Figure 5.

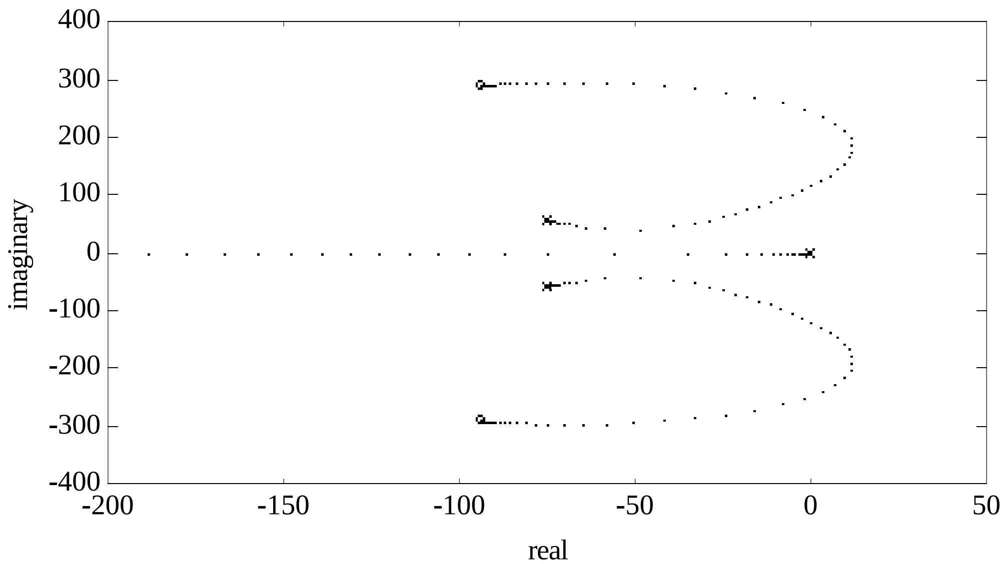

Figure 7: Root locus for the fourth order plant model under proportional gain explicit force control with $-1 \leq K_{fp} < \infty$

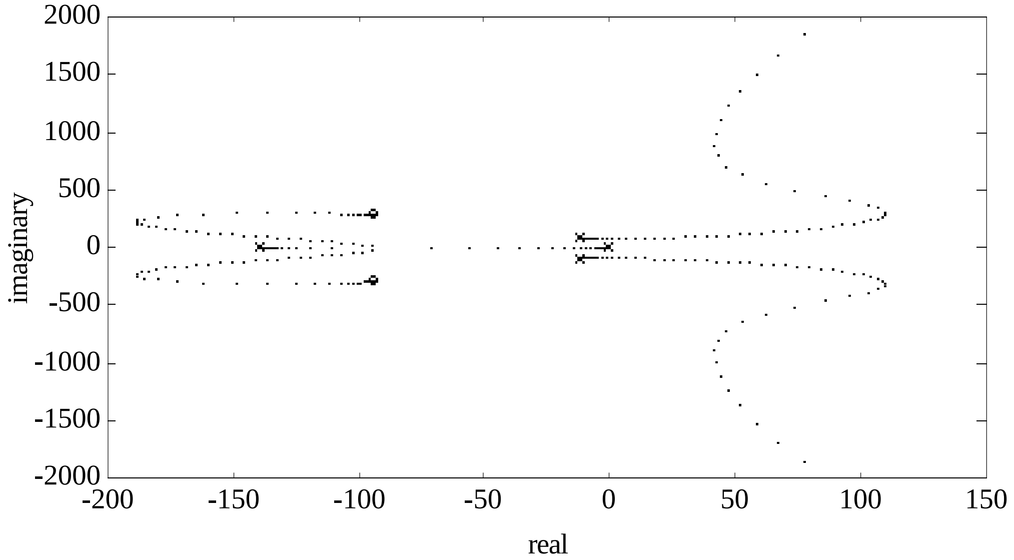

Figure 8: Root locus for the fourth order model under integral gain explicit force control.

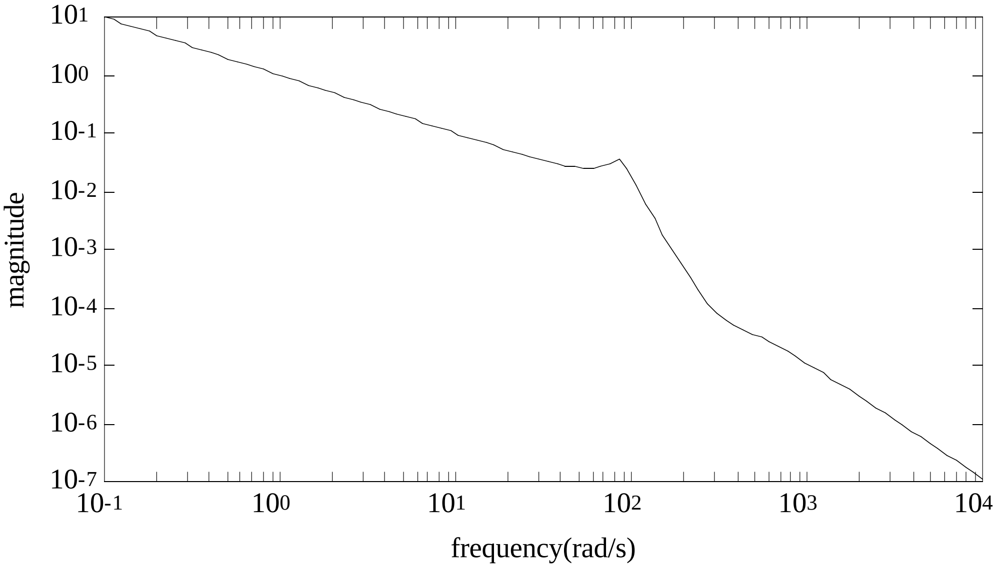

Figure 9: Bode plot for the fourth order system under integral gain explicit force control. The resonance peak corresponds to the natural frequency of the environment, but remains under a magnitude of one for gains of ~ 10. The gain margin is 28 at $\omega = 85$rad/s, which corresponds to the root locus crossing to the right half plane in Figure 8.

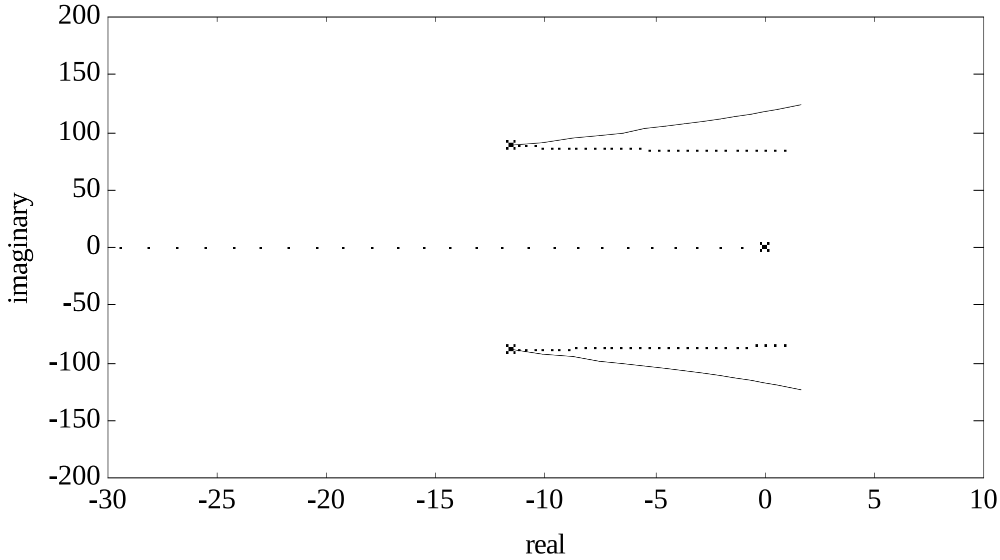

Figure 10: Comparison of proportional (solid) and integral (dotted) gain root loci. The proportional gain is in the range $0 \leq K_{fp} \leq 1.5$. The integral gain is in the range $0 \leq K_{fi} \leq 30$.

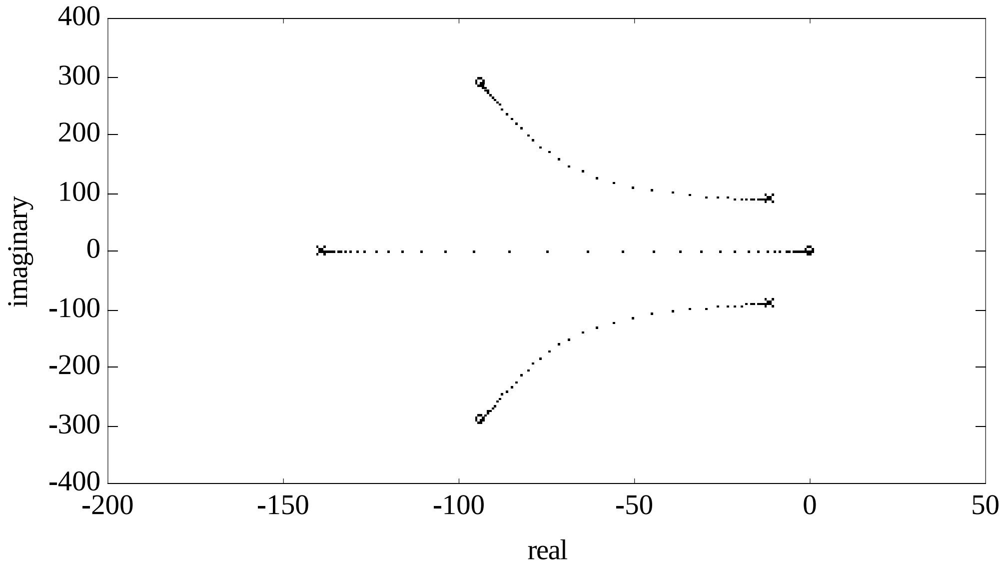

Figure 11: Root locus for the fourth order model under derivative gain explicit force control.

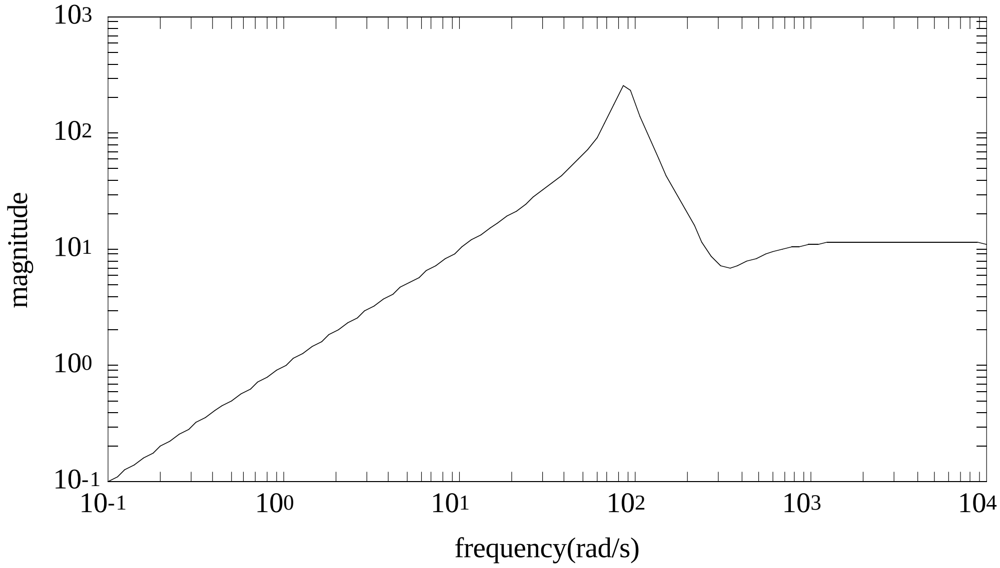

Figure 12: Bode plot for the fourth order system under derivative gain explicit force control. The resonance peak corresponds to the natural frequency of the environment. Thus, this controller acts as a band pass filter for the resonant frequency of the system.

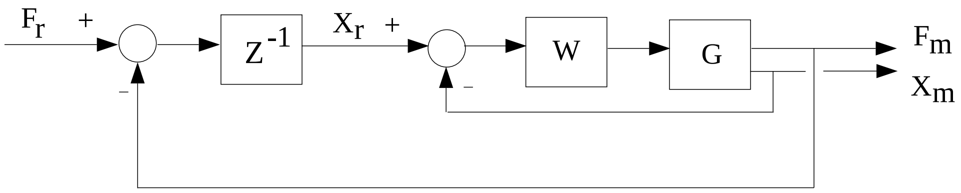

Figure 13: Block diagram of a generic position-based, explicit force controller.

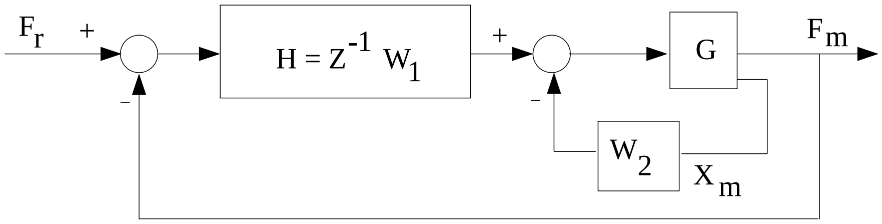

Figure 14: Reformulation of the block diagram of generic position-based, explicit force controller.

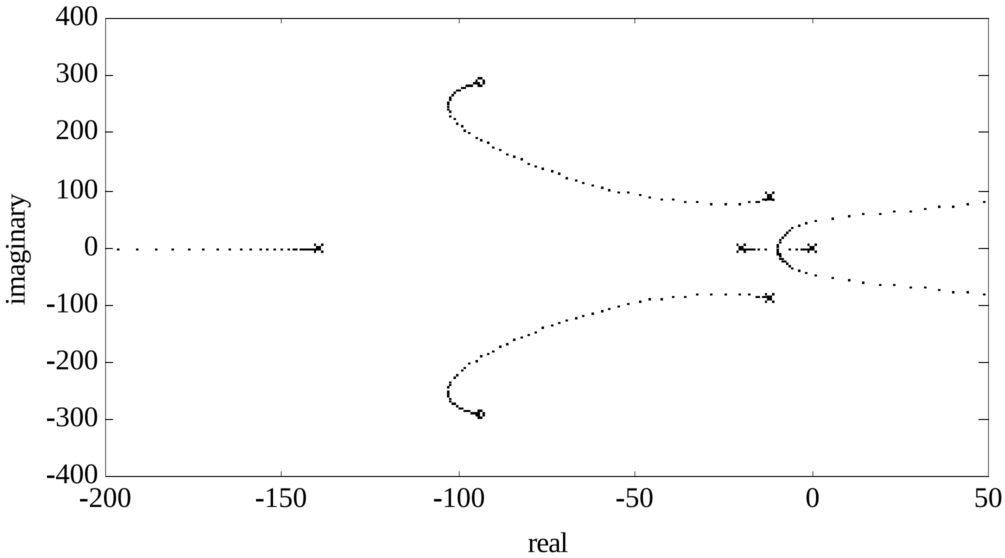

Figure 15: Root locus for the fourth order model under explicit force control with a second order lowpass filter. The poles quickly leave the real axis near the origin (for $K_f \approx 100$) and then move more slowly.

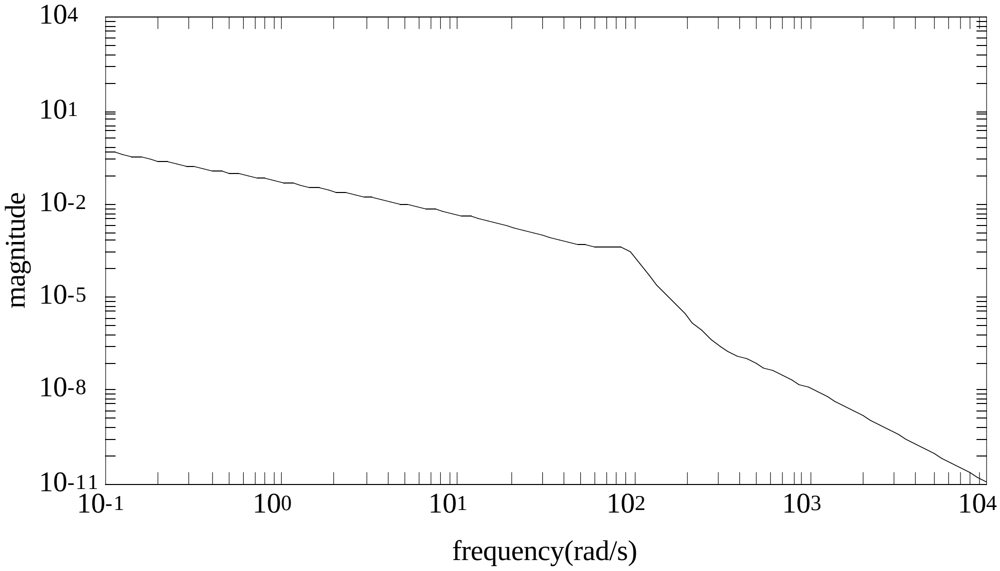

Figure 16: Bode plot for the fourth order system under explicit force control with a second order lowpass filter. Note that the resonance peak is almost completely suppressed. The gain margin is 1854 at $\omega = 48$, which corresponds to the root locus crossing to the right half plane in Figure 15.

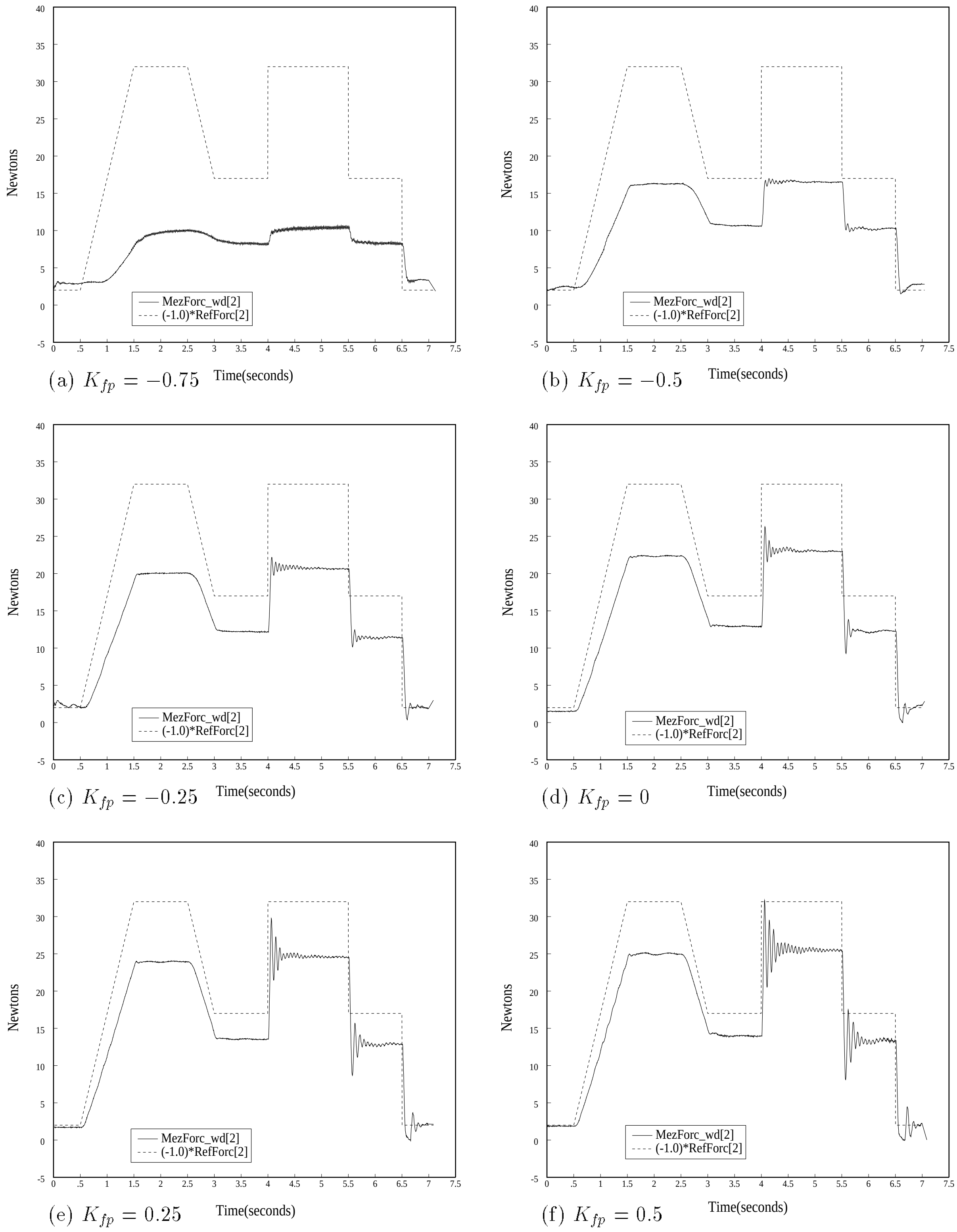

(a) $K_{fp} = -0.75$

(b) $K_{fp} = -0.5$

(c) $K_{fp} = -0.25$

(d) $K_{fp} = 0$

(e) $K_{fp} = 0.25$

(f) $K_{fp} = 0.5$

Figure 17: Experimental data of proportional gain explicit force control with feedforward. The proportional gain varies from -0.75 to 1.

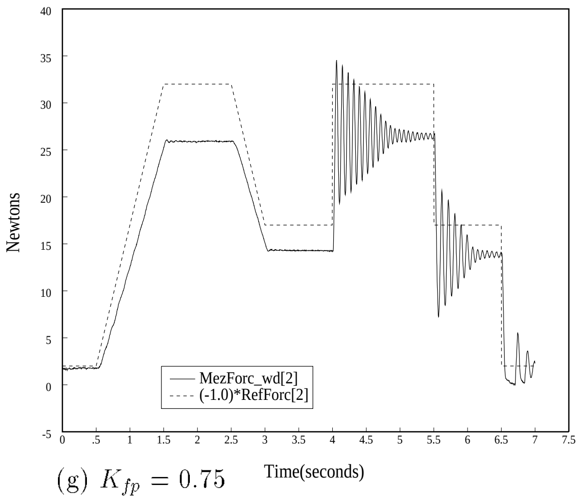

(g) $K_{fp} = 0.75$

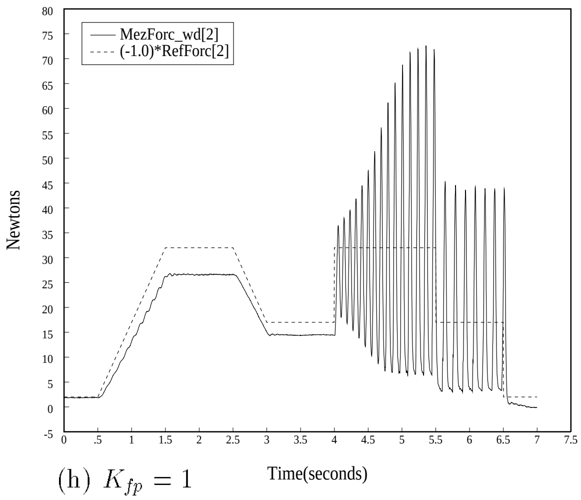

(h) $K_{fp} = 1$

Figure 17: (continued) Experimental data of proportional gain explicit force control with feedforward. The proportional gain varies from -0.75 to 1.

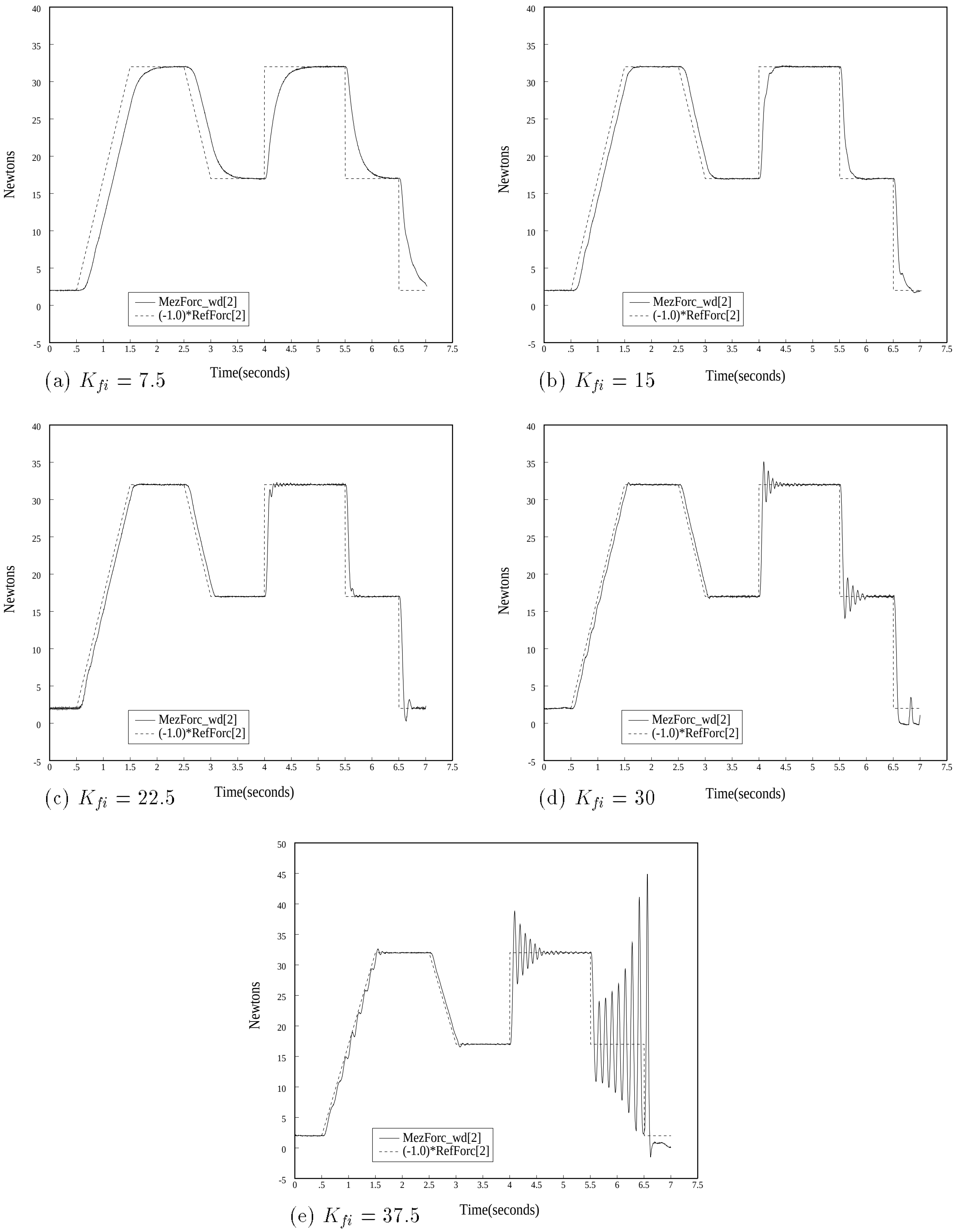

(a) $K_{fi} = 7.5$

(b) $K_{fi} = 15$

(c) $K_{fi} = 22.5$

(d) $K_{fi} = 30$

(e) $K_{fi} = 37.5$

Figure 18: Experimental data of integral gain explicit force control feedforward. The integral gain varies from 7.5 to 37.5.

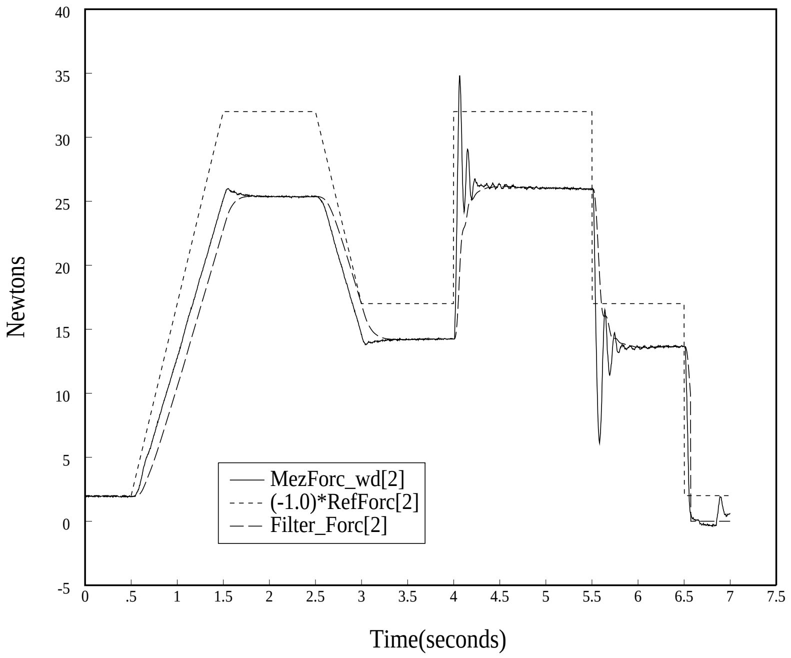

Figure 19: Experimental data from PD control with $K_{fp} = 0.5$ and $K_{fd} = 0.01$

.

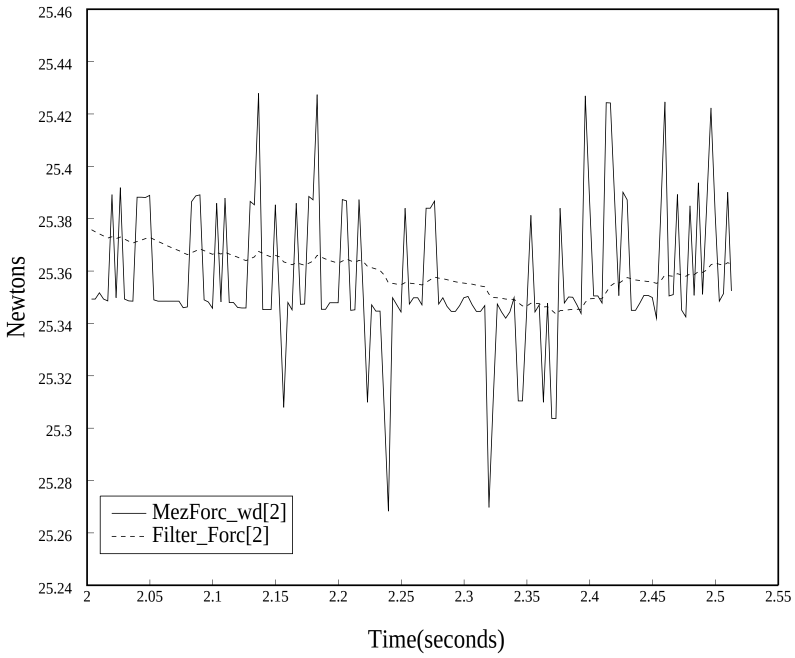

Figure 20: Filtered and unfiltered force signals for PD control.

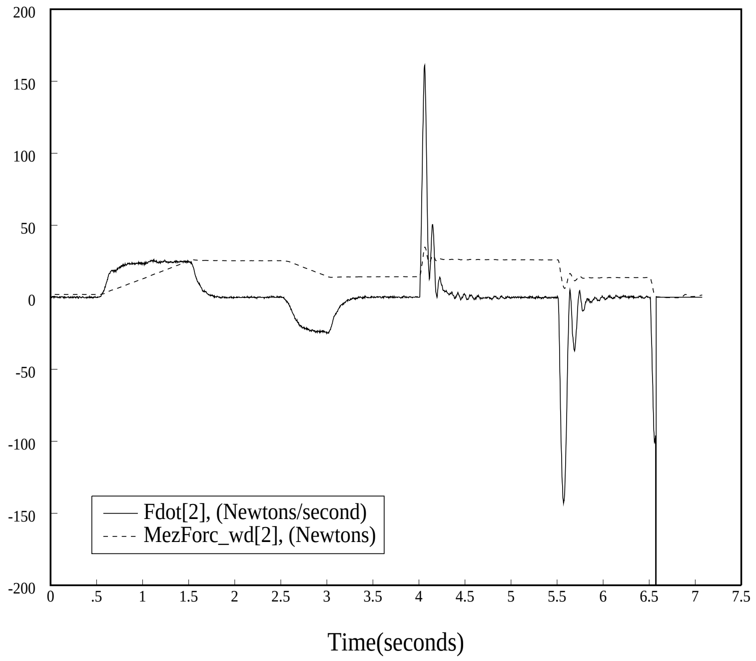

Figure 21: Calculated force derivative and measured force signal used in PD control.

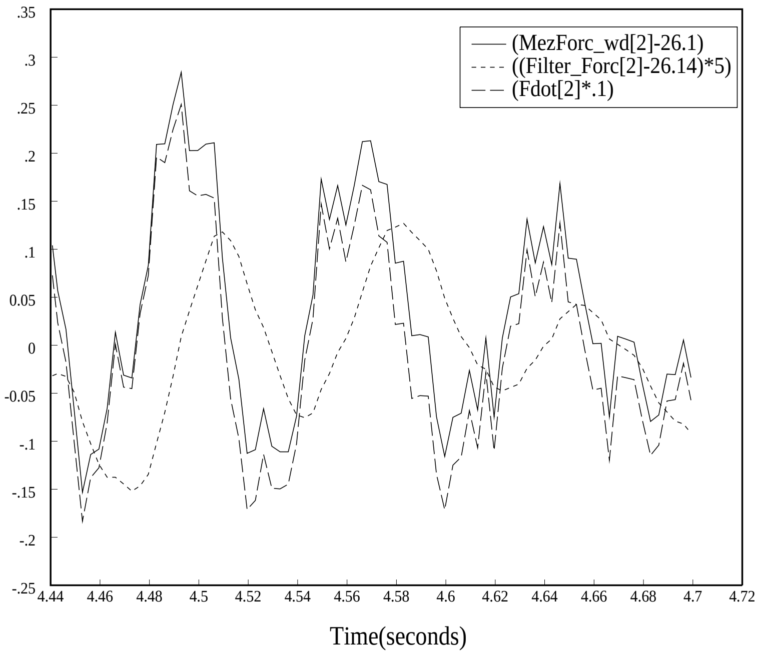

Figure 22: The lag of the filtered force causes the force derivative to be in phase with the measured force.

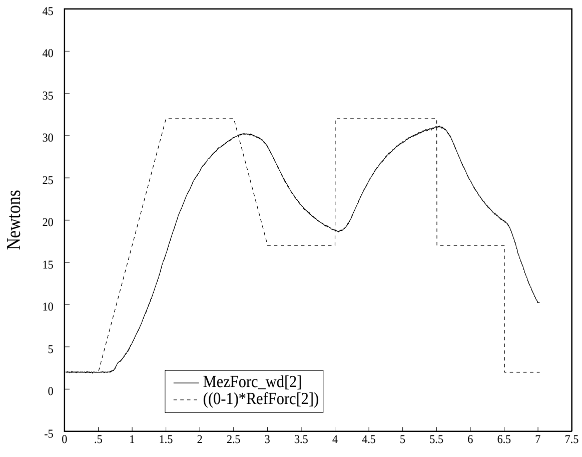

(a) $a = 15, K_{fp} = 33$

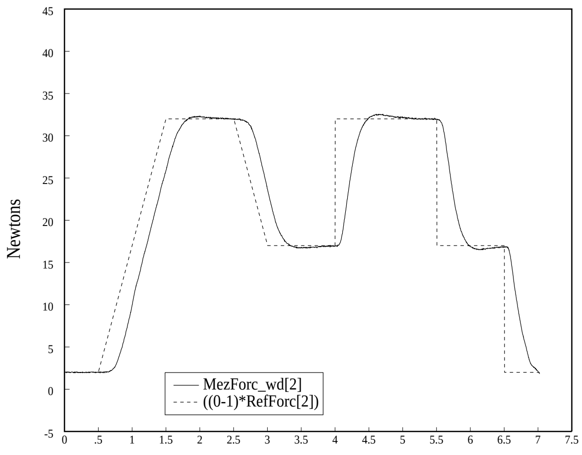

(b) $a = 15, K_{fp} = 100$

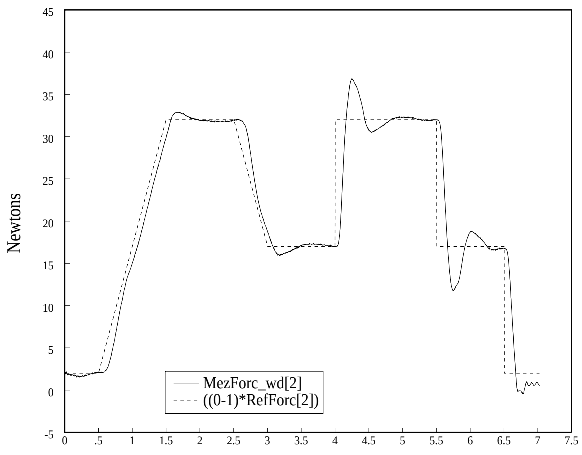

(c) $a = 15, K_{fp} = 300$

Figure 23: Experimental data of second order low pass force controller for $a = 15$, K_{fp} varied.

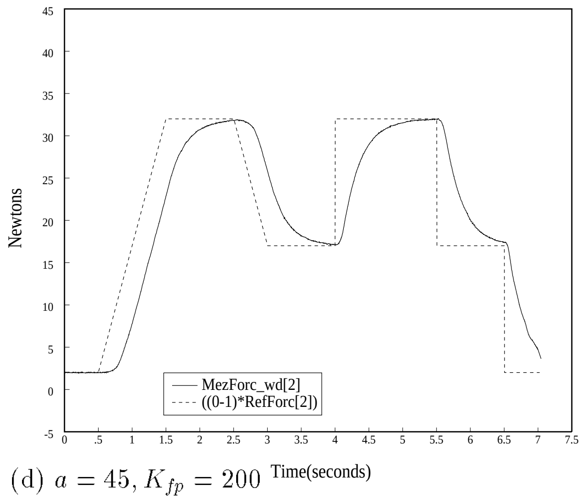

(d) $a = 45, K_{fp} = 200$

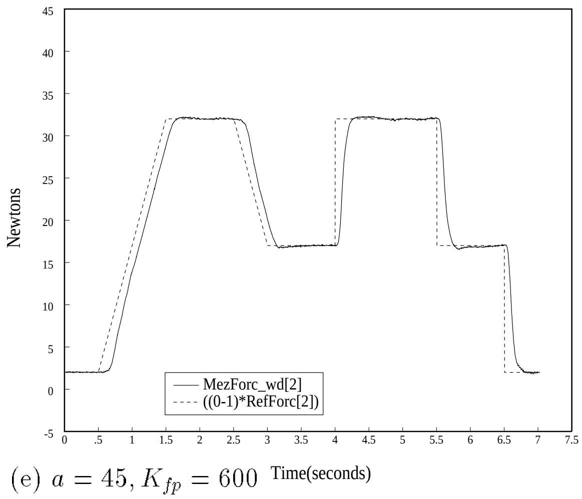

(e) $a = 45, K_{fp} = 600$

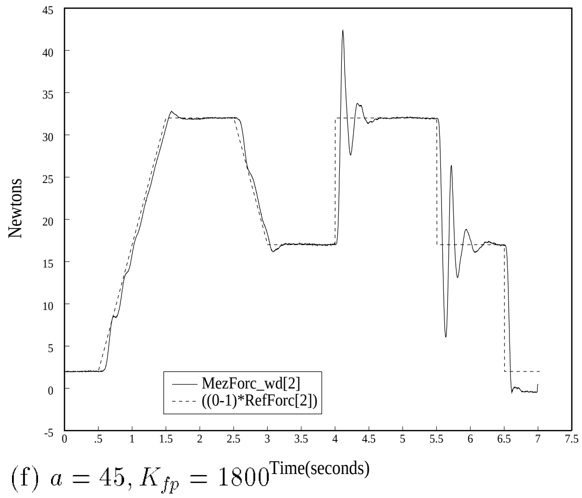

(f) $a = 45, K_{fp} = 1800$

Figure 23: (continued) Experimental data of second order low pass force controller for $a = 45$, K_{fp} varied.

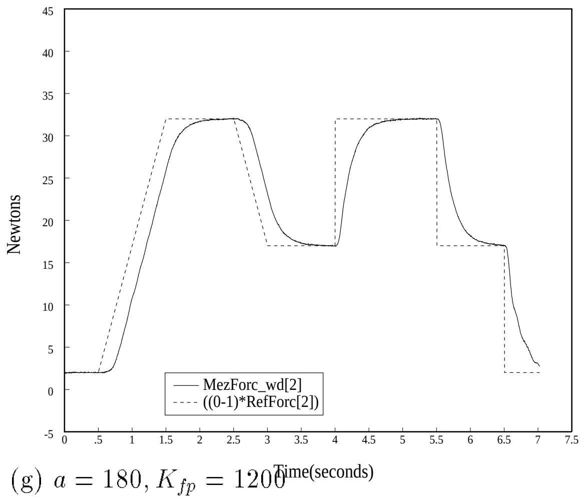

(g) $a = 180, K_{fp} = 1200$

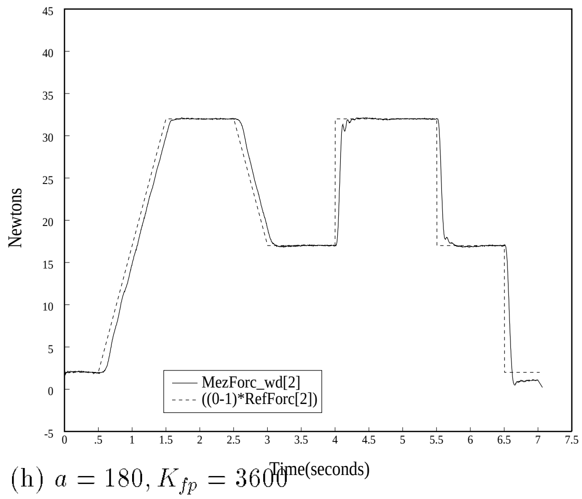

(h) $a = 180, K_{fp} = 3600$

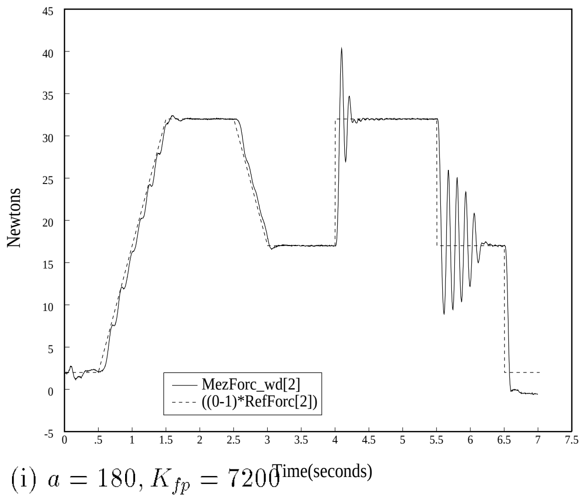

(i) $a = 180, K_{fp} = 7200$

Figure 23: (continued) Experimental data of second order low pass force controller for $a = 180$, K_{fp} varied.

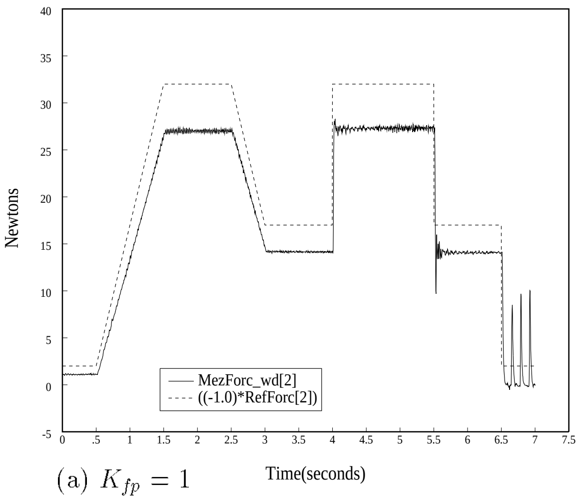

(a) $K_{fp} = 1$

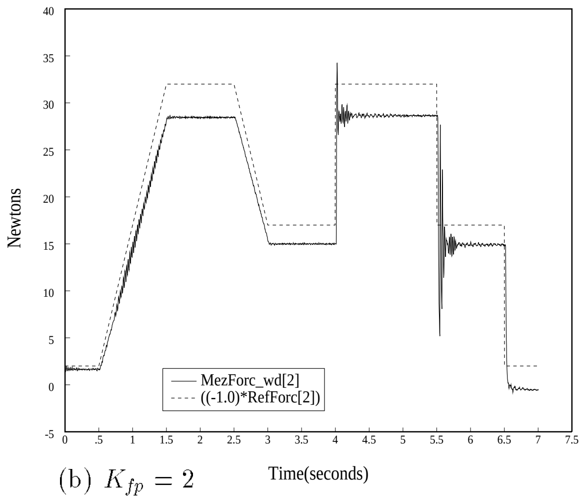

(b) $K_{fp} = 2$

Figure 24: Experimental data of proportional gain explicit force control with feedforward against the steel environment (z direction).

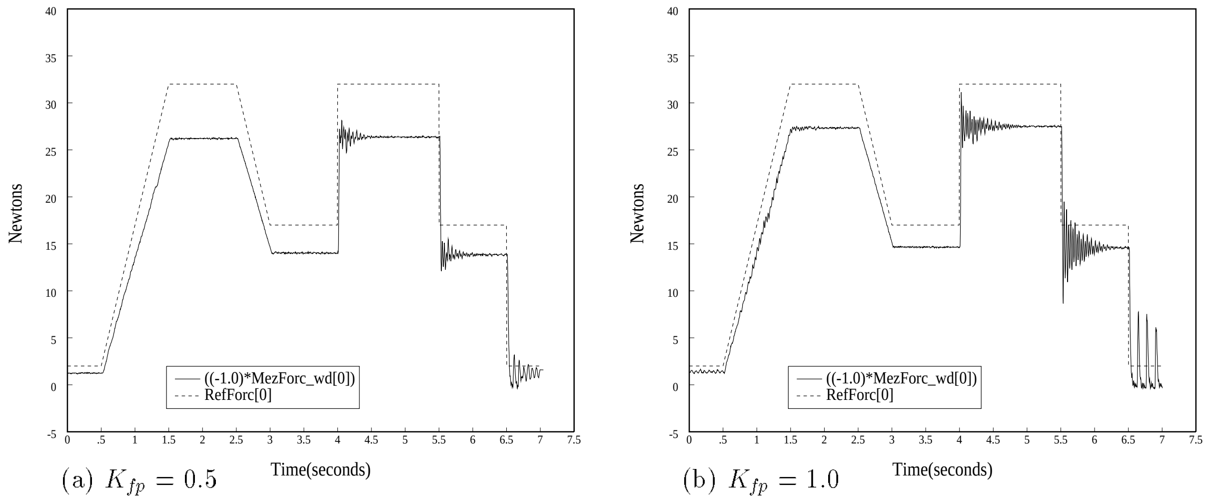

(a) $K_{fp} = 0.5$

(b) $K_{fp} = 1.0$

Figure 25: Experimental data of proportional gain explicit force control with feedforward against the steel environment (x direction).

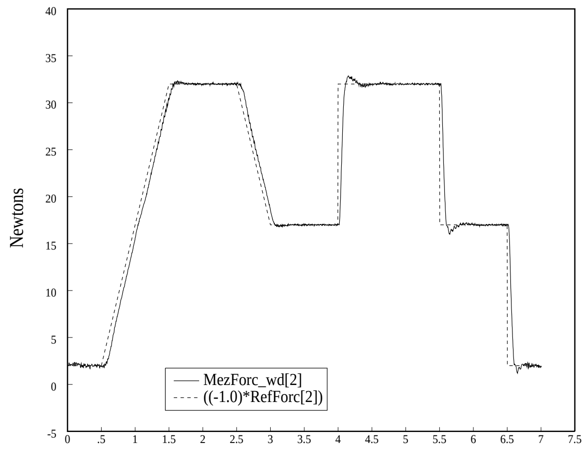

(g) $K_{fi} = 30$

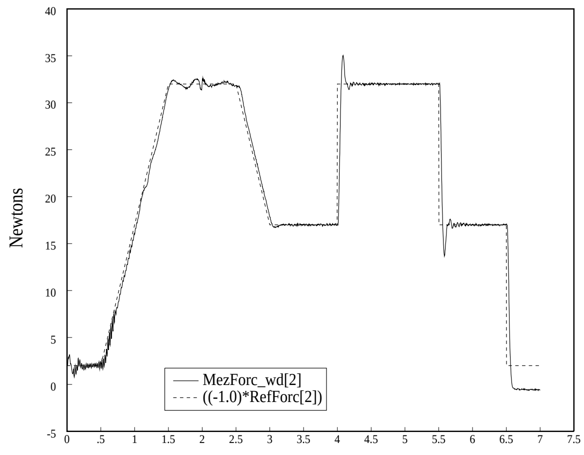

(h) $K_{fi} = 50$

Figure 26: Experimental data of integral gain explicit force control on the steel environment (z direction).

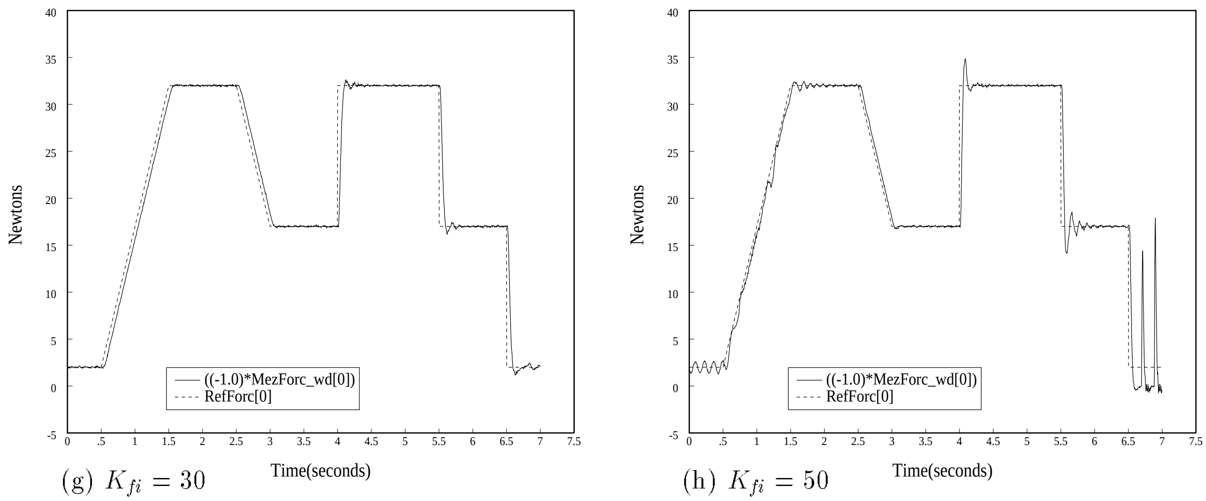

(g) $K_{fi} = 30$ (h) $K_{fi} = 50$

Figure 27: Experimental data of integral gain explicit force control on the steel environment (x direction).